Inorg. Chem. **2003**, *42*, 6300–6305

Constrained Synthesis of Cobalt Oxide Nanomaterials in the 12-Subunit Protein Cage from *Listeria innocua*

Mark Allen,[†,‡] Debbie Willits,[‡,§] Mark Young,[‡,§] and Trevor Douglas*[,†,‡]

Department of Chemistry and Biochemistry, Department of Plant Sciences, and Center for BioInspired NanoMaterials (CBIN), Montana State University, Bozeman, Montana 59717

Received April 3, 2003

The protein cage of the 12-subunit ferritin-like protein from *Listeria innocua* has been utilized as a size and shape constrained reaction environment for the synthesis of two cobalt oxide minerals, Co_3O_4 and Co(O)OH. Reaction of Co(II) with H_2O_2 at pH 8.5 under either elevated temperature (65 °C) or ambient temperature (23 °C) resulted in the formation of cobalt oxide nanoparticles encapsulated within the protein cage. At elevated temperatures, Co_3O_4 was formed while at lower temperature the oxyhydroxide Co(O)OH was found. Mineral particles, commensurate in size with the internal dimensions of the protein (5 nm), were imaged by transmission electron microscopy and shown to be surrounded by the intact protein cage. The minerals were investigated by electron diffraction and revealed a crystalline Co_3O_4 phase and an amorphous Co(O)OH phase. Further investigation of these composite materials using size exclusion chromatography, gel electrophoresis, dynamic light scattering, and ζ potential measurements indicated that the mineral was encapsulated within the protein cage giving rise to properties of both the mineral and protein components.

Introduction

The molecular level understanding of the formation of solids in biological systems has provided inspiration for the controlled formation of novel inorganic materials.[1,2] In biomineralization, self-organization of organic based templates provides scaffolding for the assembly of inorganic materials. The interaction between organic and inorganic phases relies in part on a molecular recognition between the two phases. We have previously shown that protein cages, including viruses devoid of their nucleic acid, can be used for the size dependent encapsulation of non-native materials.[3−5] The host−guest relationship between these protein cages and the encapsulated material is based primarily on a complementary electrostatic interaction. Charged interfaces play important roles in defining electrostatically distinct environments for spatially defined encapsulation. The electrostatic interactions can be approximated by Guoy−Chapman theory of charged interfaces. The electrostatic potential at a charged interface aggregates oppositely charged ions at the surface, and this high concentration of counterions drops off exponentially with distance from the surface until reaching bulk concentration.[6] These interactions are proposed at the interior of protein cages such as ferritin and viruses.[3,7] In addition, altering the chemical nature of the protein cage has been shown to significantly alter the synthetic utility of the cages.[5] A minimal set of criteria for spatially constrained nanoparticle synthesis includes a cagelike architecture to spatially constrain the size and shape of the mineral particle, chemically or electrostatically distinct interior and exterior surfaces, and the ability of small molecules to access the interior surfaces. In principle, any protein cage with a highly charged interior surface with pores that allow molecular access to the inside of the protein could act as a constrained reaction vessel.

The ferritin-like protein (FLP) cage from the bacterium *Listeria innocua* is composed of 12 identical 18 kDa subunits,

* To whom correspondence should be addressed. E-mail: tdouglas@chemistry.montana.edu.
[†] Department of Chemistry and Biochemistry.
[‡] Center for BioInspired NanoMaterials (CBIN).
[§] Department of Plant Sciences.

(1) *Biomimetic Materials Chemistry;* Mann, S., Ed.; VCH Publishers: New York, 1996.
(2) Aizenberg, J.; Grazul, J. L.; Muller, D. A.; Hamann, D. R. *Science* **2003**, *299*.
(3) Douglas, T.; Young, M. *Nature* **1998**, *393*, 152.
(4) Douglas, T.; Young, M. *Adv. Mater.* **1999**, *11*, 679.
(5) Douglas, T.; Strable, E.; Willits, D.; Aitouchen, A.; Libera, M.; Young, M. *Adv. Mater.* **2002**, *14*, 415.
(6) Stafiej, J.; Dymitrowska, M.; Badiali, J. P. *Electrochim. Acta* **1996**, *41*, 2107.
(7) Douglas, T.; Stark, V. T. *Inorg. Chem.* **2000**, *39*, 1828.

10.1021/ic0343657 CCC: $25.00
Published on Web 09/03/2003

Figure 1. Ribbon diagram of *L. innocua* FLP looking down the 3-fold channel (pdb file:1qgh[10]).

which self-assemble into an empty cage having 23 symmetry (Figure 1).[8−10] Structural analysis indicates that (0.8 nm) pores at subunit interfaces in the protein cage should allow molecular access to the interior.[10] This empty protein cage has an outer diameter of 8.5 nm and an inner diameter of 5 nm (Figure 1). This ferritin-like protein is atypical compared to the majority of structurally characterized ferritins, which assemble from 24 subunits to give a cage with an outer diameter of 12 nm and an inner diameter of 8 nm. Thus, the *L. innocua* FLP has a cavity a little more than half the diameter of the 24-subunit ferritin protein cage. The X-ray crystal structure suggests that six clusters of acidic residues on the interior surface could act as analogues of the mineral nucleation sites in ferritin. Utilizing this electrostatically distinct feature, we have previously used the *L. innocua* FLP cage for biomimetic synthesis of iron-oxide-based nanomaterials.[13] Here we report on the use of the *L. innocua* FLP for the size constrained synthesis of two cobalt oxide phases Co(O)OH and Co_3O_4 using the non-native metal ion Co(II) as a starting material. Co oxide nanomaterials with well-defined morphology and composition are finding applications as magnetic[11] and catalytic materials.[12] Our biomimetic approach to metal oxide nanoparticle synthesis allows access to well formed materials under mild synthetic conditions.

Experimental Section

Materials. All chemicals were purchased from Sigma-Aldrich and used as received with no further purification. All water used was purified through a Nanopure system to 18 MΩ resistivity.

***Listeria* Ferritin-like Protein Expression and Purification.** The *L. innocua* FLP was expressed and purified to homogeneity from an *E. coli* expression system as previously described.[13]

Co_3O_4 Mineralization. A solution of *L. innocua* FLP (15 mL, 5 mg, 2.3×10^{-5} mmol in 0.1M NaCl) was added to a jacketed reaction vessel under N_2 (to maintain an oxygen free environment). The temperature was brought up to 65 °C by flowing water through the jacketed flask, and the pH was brought to 8.5 using 50 mM NaOH (Brinkmann 718 AutoTitrator). For a cobalt loading factor of 400 Co per protein cage, 8.3×10^{-3} mmol of Co^{2+} was added to 5 mg of the protein in 15 mL reaction volume. Deaerated solutions of $Co(NO_3)_2 \cdot 6H_2O$ (12.5 mM, 0.727 mL) and the oxidant, H_2O_2 (12.5/3 mM, 0.727 mL), were added continuously and simultaneously at a constant rate (0.048 mL/min) using a syringe pump (Kd Scientific). Solutions of H_2O_2 were freshly prepared, and the concentration was determined using a permanganate titration.[14] H^+ generated during the reaction was titrated dynamically with a Brinkmann 718 automatic titrator using 50 mM NaOH. Metal ion and oxidant solutions were added over various time periods including 1, 5, 10, and 15 min, and the reaction was considered complete 15 min after addition.

Co(O)OH Mineralization. A solution of the *L. innocua* FLP (15 mL, 5 mg, 2.3×10^{-5} mmol in 0.1 M NaCl) was adjusted to pH 8.5 with 0.05 M NaOH. At room temperature (23 °C), solutions of $Co(NO_3)_2 \cdot 6H_2O$ (12.5 mM, 0.727 mL, 8.3×10^{-3} mmol) and H_2O_2 (12.5/2 mM, 0.727 mL, 4.15×10^{-3} mmol) were added continuously and simultaneously at a constant rate (0.006 mL/min) via syringe pump over a 2 h period. The reaction was run unbuffered at pH 8.5, and the H^+ generated during hydrolysis was titrated dynamically with a Brinkmann 718 STAT autotitrator (50 mM NaOH).

Characterization. Transmission Electron Microscopy (TEM). TEM data were collected on a Leo 912, with Ω filter, operating at 80 keV. Samples were concentrated using microcon ultrafilters (Microcon YM-100) with 100 kDa M_w cutoff and transferred to carbon coated copper grids. Samples were imaged stained with uranyl acetate and unstained. Electron diffraction data were collected on these samples, and *d*-spacing was calculated and compared to powder diffraction files for Co(O)OH[15] and Co_3O_4[16] after calibration of the instrument with a Au standard. Electron energy loss spectroscopy (EELS) was measured to determine elemental composition and compared to reference spectra.

Dynamic Light Scattering (DLS) and ζ Potential. Dynamic light scattering (DLS) and ζ potential measurements were made on a Brookhaven Instruments *ZetaPals* (phase analysis light scattering) particle size/ζ potential analyzer. DLS was measured at 90° using a 661 nm diode laser, and the correlation functions were fit using a non-negatively constrained least-squares analysis.[17] ζ potential was measured by applying a 7.10 V/cm ac field and measuring sample mobility at 25 °C. The data were fit using a Smoluchowski data analysis.[18]

Polyacrylamide Gel Electrophoresis (PAGE). PAGE was performed under native nondenaturing conditions using a 5% native polyacrylamide gel. Gels were stained for protein using Coomassie blue and stained for Co using 1-nitroso-2-naphthol.[7,19]

(8) Bozzi, M.; Mignogna, G.; Stefanini, S.; Barra, D.; Longhi, C.; Valenti, P.; Chiancone, E. *J. Biol. Chem.* **1997**, *272*, 3259.
(9) Stefanini, S.; Cavallo, S.; Benedetta, M.; Chiancone, E. *Biochem. J.* **1999**, *338*, 71.
(10) Ilari, A.; Stefanini, S.; Chiancone, E.; Tsernoglou, D. *Nat. Struct. Biol.* **2000**, *7*, 38.
(11) Skumryev, V.; Stoyanov, S.; Zhang, Y.; Hadjipanayis, G.; Givord, D.; Nogues, J. *Nature* **2003**, *423*, 850.
(12) Jansson, J.; Palmqvist, A. E. C.; Fridell, E.; Skoglundh, M.; Osterlund, L.; Thormahlen, P.; Langer, V. *J. Catal.* **2002**, *211*, 387.
(13) Allen, M.; Willits, D.; Mosolf, J.; Young, M.; Douglas, T. *Adv. Mater.* **2002**, *14*, 1562.
(14) Nedoloujko, A.; Kiwi, J. *J. Photochem. Photobiol., A* **1997**, *110*, 149.
(15) Powder Diffraction File 07-0169 (Heterogenite Co(O)OH), Joint Committee on Powder Diffraction Standards, Swarthmore, PA.
(16) Structure File 9362 (Co_3O_4), Inorganic Crystal Structure Database, Karlsruhe, Germany.
(17) Finsy, R. *Adv. Colloid Interface Sci.* **1994**, *52*, 79.
(18) Tscharnuter, W. W. *Appl. Opt.* **2001**, *40*, 3995.
(19) Wünsch, G. *Talanta* **1979**, *26*, 177.

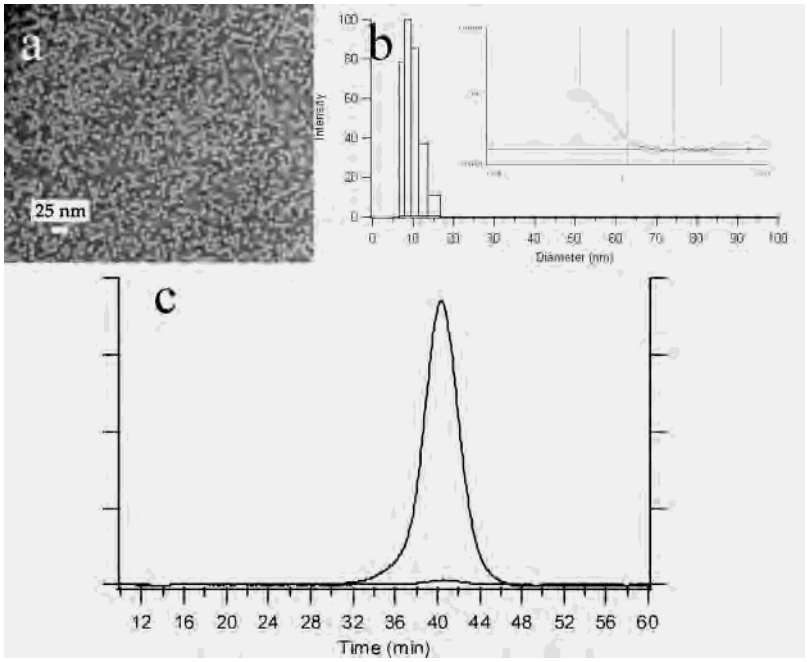

Figure 2. (a) Transmission electron micrograph of *L. innocua* FLP negatively stained with uranyl acetate. (b) Dynamic light scattering of empty *L. innocua* FLP indicating a diameter of 9 nm (inset is the corresponding correlation function). (c) Size exclusion chromatography of empty *L. innocua* FLP measuring absorbance at 280 and 350 nm.

Size Exclusion Chromatography (SEC). SEC was performed on a Biologic Duo-Flow fast protein liquid chromatography system equipped with a quad-tech UV−vis detector and using a superose 6 (Amersham Pharmacia) size exclusion chromatography column.

UV−Vis Spectroscopy. UV−vis absorbance data were measured on an Agilent 8453 spectrophotometer equipped with a diode array detector.

Results and Discussion

Purified *L. innocua* FLP provides a unique size constrained reaction environment for the synthesis of Co oxide based nanomaterials. The purified, recombinant protein self-assembled readily into the 8.5 nm cagelike architecture particles indistinguishable from the native protein. This was confirmed by transmission electron microscopy, which revealed protein cages of 8.5 nm diameter (Figure 2 a). Dynamic light scattering indicated a particle size of 9.2 ± 0.4 nm diameter (Figure 2b), and elution from size exclusion chromatography (Figure 2c) was consistent with a protein of approximately 220 kDa. The formation of this monodispersed cagelike architecture is required for the size constrained encapsulation of the metal oxide particles. Dynamic light scattering of the unmineralized protein cages showed no significant change in particle diameter at temperatures of 65 °C. Typically, the purified FLP cages were treated with aliquots of Co(II), under an atmosphere of N_2, at pH 8.5, and were oxidized with H_2O_2 under either room temperature (23 °C) or elevated temperature (65 °C). In the presence of the empty FLP cages, both ambient and high temperature reactions proceeded to form homogeneous olive green solutions. In contrast, reactions in the absence of the FLP cages resulted in the bulk precipitation of olive green solids. The lack of precipitate in the reactions containing the FLP cage, and the strong color present in these solutions, suggested that the oxidative hydrolysis of Co(II) occurred in a spatially selective manner within the confines of the protein cage.

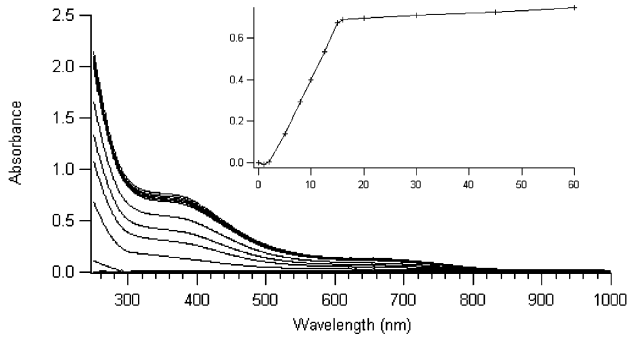

Figure 3. Time course for the synthesis of Co_3O_4−FLP (15 min reagent addition), monitored by UV−vis spectroscopy. The inset shows the change in absorbance at 350 nm with time (min).

The reactions could be followed by monitoring the change in the visible absorbance (Figure 3) or by dynamic titration of H^+ generated during the oxidative hydrolysis (reactions 1 and 2). Comparison of the measured change in absorbance at 350 nm shows that the rate of Co(II) oxidation in the presence of the protein cage was limited by the rate of substrate addition at both temperatures tested (Figure 3 inset). The products formed appeared to be independent of the rate of cobalt and oxidant addition from 0.6 to 9 μmoles/min. Titration of H^+ generated during the reaction revealed an identical behavior, confirming that mineral formation is directly coupled to the oxidative hydrolysis (data not shown) and the rate of reaction is limited by substrate addition.

$$3Co^{2+}(aq) + H_2O_2(aq) + 2H_2O(l) \xrightarrow{65\ ^\circ C} Co_3O_4(s) + 6H^+(aq) \quad (1)$$

$$2Co^{2+}(aq) + H_2O_2(aq) + 2H_2O(1) \xrightarrow{25\ ^\circ C} 2Co(O)OH(s) + 4H^+(aq) \quad (2)$$

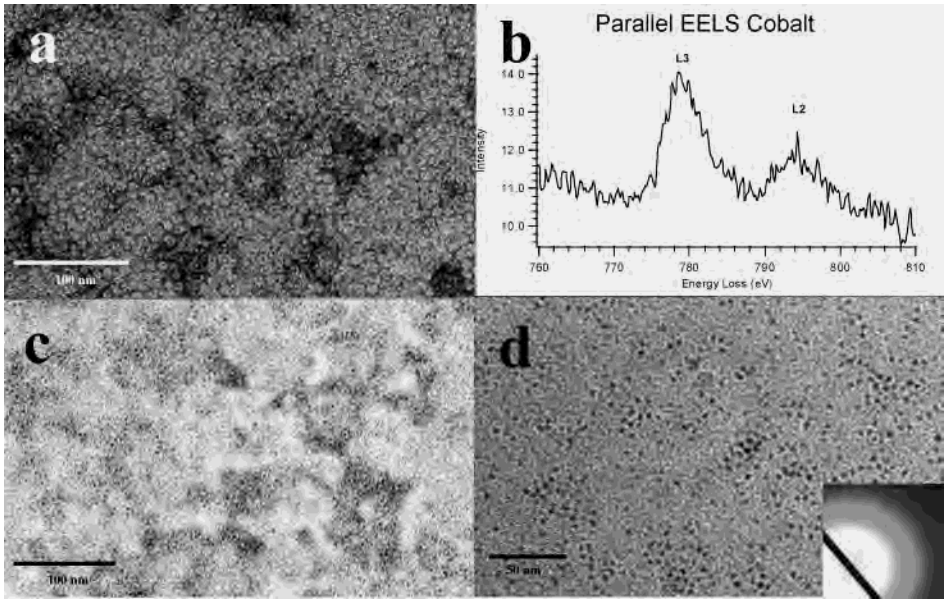

Figure 4. (a) Transmission electron micrographs of Co(O)OH−FLP negatively stained with uranyl acetate. (b) Electron energy loss spectrum of Co_3O_4−FLP showing the L3,2 absorption of cobalt. (c) TEM of Co_3O_4−FLP stained with uranyl acetate. (d) TEM of Co_3O_4−FLP unstained, inset is the electron diffraction data collected from Co_3O_4−FLP.

The products of mineralization were characterized by transmission electron microscopy (TEM), electron diffraction, electron energy loss spectroscopy (EELS), dynamic light scattering (DLS), ζ potential, size exclusion chromatography (SEC), UV−vis spectroscopy, and native polyacrylamide gel electrophoresis (PAGE). For all characterizations, the mineralized protein was directly compared with the unmineralized protein to assess the spatial selectivity of the mineralization reactions. Together, these characterizations have allowed us to answer the question of whether mineralization occurred on the inside or outside of the protein cage.

The products of the mineralization reactions were visualized by TEM. Both preparations of mineralized FLP (high and ambient temperature syntheses) were negatively stained with uranyl acetate (Figure 4a,c) and demonstrated the intact protein cages. For mineralization reactions performed at elevated temperatures, clear electron dense cores of a size consistent with the interior dimensions of the protein cage were observed (Figure 4d). The particle size was measured and found to be quite monodisperse with an average diameter of 4.34 ± 0.55 nm. This is consistent with the interior dimensions of the FLP cage, which defines an interior cavity of approximately 5 nm diameter. However, the products of similar reactions performed at room temperature did not show clear electron dense particles. This difference is likely the result of a difference in particle crystallinity, which would result in differences in the Bragg scattering and subsequent contrast between the samples. A higher temperature synthesis is expected to be responsible for the removal of structural waters that would be present in the room temperature synthesis while the mineral structure is expected to be significantly influenced by the stoichiometry of oxidant to metal. Kinetics were measured qualitatively on the two syntheses and clearly showed a considerably faster reaction for the high temperature reaction, probably the direct result of overcoming the energy barrier of nucleation. Measurements of electron diffraction indicated that the material formed at high temperature was crystalline (Figure 4d inset) while the low temperature synthesis yielded no clear diffraction pattern, consistent with a poorly crystalline mineral. Selected area diffraction of a large number of particles, from the high temperature synthesis, revealed a powder pattern that yielded *d*-spacings (Table 1) which match well with the reported values of the spinel phase of cobalt oxide Co_3O_4 (Table 1).[15] No diffraction pattern could be distinguished from the product of the room temperature synthesis in the presence of the FLP. This is similar to the Co(O)OH mineralization of the 24-subunit ferritin under similar conditions which showed weak diffraction and poorly defined mineral cores.[7] The material from the room temperature synthesis is in all likelihood amorphous while that of the higher temperature synthesis is expected to be crystalline. The products of both syntheses were washed thoroughly with water and analyzed by EELS, confirming that the FLP was mineralized with a cobalt oxide material, as evidenced by the 778 and 794 eV L3,2 absorptions (Figure 4b). Control reactions, run in the absence of protein cage, resulted in the bulk precipitation of dark green solids for both the reaction conditions. The bulk precipitate from the reaction at elevated temperature showed a powder diffraction pattern (electron diffraction, *d*-spacings = 0.243, 0.203, and 0.146 nm) consistent with the spinel phase, Co_3O_4,[16] while that of the low temperature reaction gave a broad diffraction with *d*-spacings of 0.44, 0.24, and 0.18 nm (Supporting Information) consistent with Co(O)OH, the mineral heterogenite.[15]

Table 1. *d*-Spacing for Co_3O_4 and Measured *d*-Spacing for 65 °C Reaction in Listeria FLP

d-spacing	measured *d*	(*hkl*)
0.2432	0.24	311
0.2016	0.20	400
0.155		333
0.1426	0.14	044

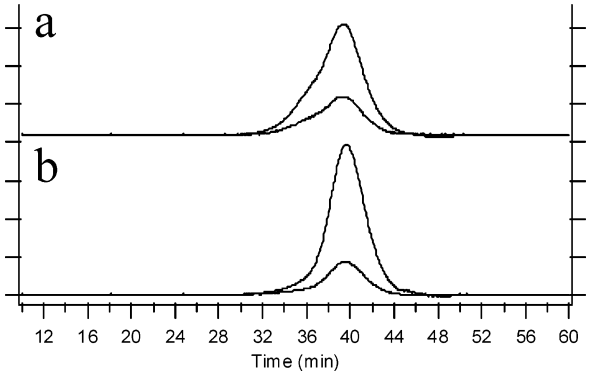

Figure 5. Size exclusion chromatography of mineralized *L. innocua* FLP cages. Elution was monitored at both 280 nm (protein) and 350 nm (Co oxide mineral), confirming the composite nature of the mineralized protein cage. Elution times for the mineralized and unmineralized protein cages were identical. (a) Room temperature synthesis of Co(O)OH−FLP. (b) High temperature synthesis of Co_3O_4−FLP.

The composite nature of the mineralized protein cage was analyzed by UV−vis spectroscopy, size exclusion chromatography, dynamic light scattering, and gel electrophoresis. The UV−vis spectrum of the mineralized protein revealed broad absorption centered at 350 nm consistent with O → Co(III) charge transfer band (Figure 3). This was in addition to strong absorption at 280 nm due to the protein. In contrast, protein cages prior to mineralization showed no absorption at 350 nm. As shown in Figure 5, elution of the mineralized protein cages on size exclusion chromatography was monitored by both the absorbance due to the protein (280 nm) and by absorbance due to the mineral particle (350 nm). For the products of both mineralization reactions, the elution profile indicated coelution of the protein cage and the mineral particle from the column with a retention time identical to that of the empty *L. innocua* FLP cage (Figure 2c). This coelution indicates the composite (protein−mineral) nature of the product and also suggests that the overall structure of the protein cage has not been significantly perturbed by the synthesis. Size exclusion chromatography is sensitive to relatively small differences in particle size, and these data suggest that the mineral and protein phases are intimately associated. This also indicates that in both reactions the protein cage architecture encapsulates the mineral particle illustrating the spatial selectivity of these reactions.

Dynamic light scattering of the unmineralized FLP indicated a cage of 9.2 ± 0.4 nm diameter with a narrow size distribution (Figure 2b). After mineralization at either room temperature or elevated temperature, there was no significant difference in the observed correlation function. When fit using a non-negatively constrained least squares (NNLS) analysis, these data indicated a population with mean diameter of 9.3 ± 0.6 nm for the room temperature reaction and 9.2 ± 0.8 nm for the reaction at elevated temperature (Figure 6). Within the limits of this technique, it appears that the diameter of the cage remained unaltered during these reactions suggesting that all mineralization had occurred within the confines of the protein cage. Electrophoresis was used to further probe the composite nature of the products of the mineralization reactions.

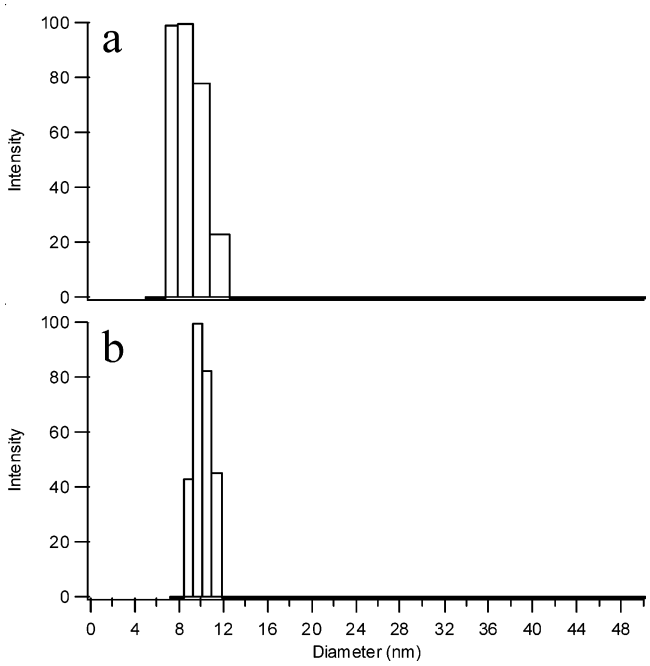

Figure 6. Dynamic light scattering of mineralized FLP. (a) Room temperature synthesis of Co(O)OH. (b) High temperature synthesis of Co_3O_4.

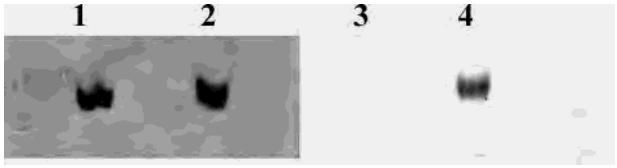

Figure 7. Native gel electrophoresis of *L. innocua* FLP on 5% PAGE. Coomassie stain of (1) unmineralized and (2) Co_3O_4 mineralized *L. innocua* FLP cages, and 1-nitroso-2-naphthol stain of (3) unmineralized and (4) Co_3O_4 mineralized *L. innocua* FLP cages.

Both the empty *L. innocua* protein cage and preparations of Co oxide mineralized protein cages were electrophoresed on 5% polyacrylamide gels under native (nondenaturing) conditions. Gels were selectively stained for Co using 1-nitroso-2-naphthol (25 mM in 1:1 H_2O/MeOH)[7] and for protein using Coomassie blue. Both preparations of the mineralized *L. innocua* FLP cages stained with 1-nitroso-2-naphthol and with Coomassie blue, while the empty protein cage stained only with the Coomassie blue (Figure 7). The comigration of the assembled *L. innocua* FLP cage in both mineralized samples and in the empty *L. innocua* FLP cage samples indicated that the mineralized cage remained intact. In addition, these data suggest that the overall charge on the exterior of the protein and the mineralized protein samples has not been measurably altered during the synthesis. This supports our assertion that mineralization occurred in a spatially selective manner and that insignificant amounts of Co deposited on the outer surface of the protein. This was additionally confirmed by measurement of the surface charge, ζ potential, of the FLP before and after mineralization. At pH 8.5, the ζ potential of the unmineralized protein was measured to be −30 ± 0.6 mV while the Co_3O_4 mineralized FLP had a ζ potential of −31 ± 0.8 mV (data not shown). The accuracy of a typical ζ potential measurement is ±2%. If cobalt ions were attached to the outside of the protein, a

more positive ζ potential would be expected. The fact that the ζ potential is slightly more negative in the mineralized protein may be due to the fact that, at pH 8.5, the surface of the mineral has a net negative charge, being above the pH_{zpc} of Co_3O_4, which is reported to be 7.3.[20]

Conclusions

Our data suggest that the *L. innocua* FLP can be used as a constrained reaction environment for the synthesis of nanomaterials using non-native substrates. Under a range of synthetic conditions, including elevated temperatures, the protein cage remains unaltered. At both room temperatures and elevated temperatures, the oxidation of Co(II) results in mineral particles which are encapsulated within the assembled protein cage.

We speculate that this high degree of spatial compartmentalization is the result of very different electrostatic interfaces present at the interior and exterior of this protein cage. This predicts that the electrostatic characteristics of the interior surface direct the mineralization of transition metal oxides and oxyhydroxides. Gouy−Chapman theory can be used to rationalize the aggregation of counterions at the interior protein interface. This suggests that, in the *L. innocua* FLP cage, cations, such as Co(II), will aggregate along the charged interior of the protein cage resulting in a nucleation event by clustering Co(II/III) cations at the interface. It is also possible that this high local concentration at the protein−solution interface lowers the redox potential of Co(II) oxidation and thus facilitates spatially selective oxidation. As in mammalian ferritin biomineralization, after nucleation, the initially formed crystallite can act as a catalytic site for further oxidative hydrolysis. Therefore, the mineralization process within the protein cage is autocatalytic for mineralization of the mineral oxide and affords a high level of control in the synthesis of size constrained particles.

The synthesized materials are both size and shape constrained by the inner volume of the protein cage. Clearly, small molecules must have access from the bulk to the interior of the protein cage through pores at the subunit interfaces. Oxidative hydrolysis selectively entraps the mineral product within the protein cage. This spatial isolation within the protein cage prevents bulk aggregation of the mineral particles and results in a stable, monodisperse colloid. Our results mimic the reactivity of mammalian ferritin, in which we have previously demonstrated the spatially selective mineralization of amorphous Co(O)OH nanoparticles. Our results suggest the potential for nanomaterial synthesis using an increasingly diverse library of protein cages as size constrained templates. The current work illustrates this synthetic approach using a uniquely sized cage that approaches the dimensions of large molecules rather than small materials. The *L. innocua* FLP allows synthesis of nanomaterials having properties different from larger protein-encapsulated materials with potential application in electronics and catalysis.

Acknowledgment. Acknowledgment is made to Sue Brumfield for assistance with TEM. This work was supported by grants from NSF (CHE-9801685) and Matsushita Electric Ind. Co. Ltd. for partial support of this research.

Supporting Information Available: Additional figure. This material is available free of charge via the Internet at http://pubs.acs.org.

IC0343657

(20) Ardizzone, S.; Spinolo, G.; Trasatti, S. *Electrochim Acta* **1995**, *40*, 2683.